

## Does Electron Spectrum Affect TLD-100 Dose Response in 6 MV Photon Beam Irradiation?

Neslihan Sarigül<sup>1,a,\*</sup>

<sup>1</sup> Institute of Nuclear Science, Hacettepe University, Ankara, Türkiye.

\*Corresponding author

### Research Article

#### History

Received: 12/03/2022

Accepted: 29/06/2022

#### Copyright



©2022 Faculty of Science,  
Sivas Cumhuriyet University

### ABSTRACT

In this study, the electron spectrum effect on the TLD-100 dosimeter response to a 6 MV photon beam in different media like water, aluminum, polystyrene, iron, copper, and lead using Monte Carlo and Burlin cavity theory was evaluated. To calculate and compare the dose to medium to dose to cavity correction factors ( $f$ ), the electronic equilibrium spectrum produced by the 6 MV photon beam and its maximum electron energy in different media were used. The electronic equilibrium spectra were obtained using Beamdp Monte Carlo Simulation. Using two different methods, the cavity theory was applied to obtain the response of the TLD-100 to 6 MV photon beam in the media considered. In the first method, the average mass collision stopping power ratios and the average mass effective attenuation coefficients were calculated using the electron spectrum of 6 MV. In the second method, these parameters were calculated based on the maximum energy value of 6 MV. The maximum difference between the  $f$  values obtained using the two methods was about 10 % for lead, while it was less than 2.5 % for other media. Consequently, the differences between  $f$  factors calculated using these two methods were insignificant except for lead.

**Keywords:** MC, LiF: MgTi, Cavity theory, Lead.

[nsarigul@hacettepe.edu.tr](mailto:nsarigul@hacettepe.edu.tr)

<https://orcid.org/0000-0002-5371-7924>

## Introduction

Thermoluminescence dosimeters (TLDs) are one of the most effective materials used to measure the absorbed dose in many fields such as medicine and industry. TLD-100 (LiF: MgTi) chip dosimeters are preferred because of their near tissue equivalence effective number, wide linear response range, and low signal fading [1,2]. Also, they have a very small size for point dose measurements. Moreover, TLD-100 can even be used for in vivo measurement of dose in proton or intraoperative electron radiation therapy [3,4]. TLD-100 detectors are constructed of a different material than the medium. This creates a cavity where the TLDs are used to measure a dose. The general cavity theory is used the relationship between the absorbed dose and the dose in the medium ( $D_{med}$ ) and the average absorbed dose in the cavity ( $D_{cav}$ ) [5].

Monte Carlo (MC) simulations report dose-to-medium. MC simulations give more realistic results, an important reason why MC is suggested to be the gold standard. Especially, in or near heterogeneities, it has been used to get an accurate estimation of absorbed dose [6–8]. In the literature, the general cavity theory was examined using MC for LiF,  $Li_2B_4O_7$ ,  $CaSO_4$ ,  $CaF_2$ , and dosimeters inside perspex, water, aluminum, copper, and lead after  $^{60}Co$  gamma rays and megavoltage photon beams exposures [9,10]. In these studies, it has been shown that the mass collision stopping-power ratio and the mass energy-absorption coefficient ratio of the water to the phantom material change more rapidly with energy in materials with high atomic numbers. The electron spectrum effect was examined on LiF for  $^{60}Co$

gamma-rays in the same media that is presented in this paper using electronic equilibrium spectra and its maximum energy [10]. However, in these studies, it was not specified how the TLD-100 dose-response was affected by the electron spectrum obtained from a 6 MV photon beam, which is frequently used in clinics.

In clinical applications, the TLD-100 dosimeter is commonly irradiated with the 6 MV photon beam. Therefore, evaluating the effect of the electron spectrum on the TLD-100 dosimeter response is necessary for the 6 MV photon beam. The main aim of the following study is to observe the electron spectrum effect on the TLD-100 response to media considered using effective mass attenuation coefficient and mass collision stopping power from electron spectrum and maximum energy of the 6 MV photon beam. In summary, the effect of electron spectrum on TLD-100 response was investigated in different densities by using MC simulation and Burlin cavity theory.

## Materials and Methods

### Monte Carlo

The Monte Carlo EGSnrc package was used for all simulations. EGSnrc/Beamnrc was used to generate phase space data, which are on the surface of slabs. The spectral distribution simulation tool in the BeamDp from phase space data was used to calculate spectrum weighted mass stopping power ratios. The phantom set-ups were created using BEAMnrc, having TLD-100 inserted into the six different

materials as shown in Fig.1. The TLD-100 chip was simulated in different depths as shown in Table 1. The placements of the TLD-100 chip were calculated using water equivalent depths and ensured that the depths were beyond the maximum depth dose ( $d_{max}$ ).

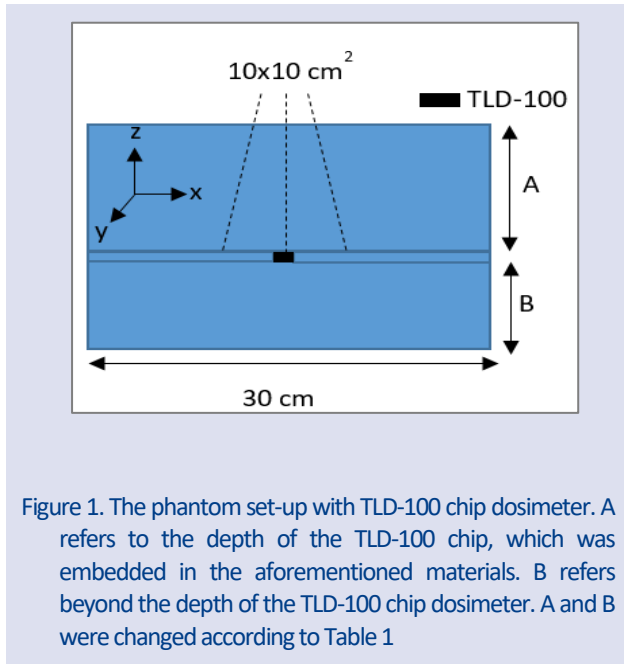


Figure 1. The phantom set-up with TLD-100 chip dosimeter. A refers to the depth of the TLD-100 chip, which was embedded in the aforementioned materials. B refers beyond the depth of the TLD-100 chip dosimeter. A and B were changed according to Table 1

The field size was 10x10 cm<sup>2</sup> and the source-axis distance (SAD) was set to 100 cm. The phantom material was chosen 30 cm cube of material. H2O700ICRU, AL700ICRU, POLYSTY700ICRU, CU700ICRU, FE700ICRU, and PB700ICRU were assigned to water, aluminum, polystyrene, copper, iron, and lead. The density of TLD-100 is 2.64 gcm<sup>-3</sup>. It consists of Li (26.70%), F (73.28%), with Mg (0.001%) and Ti (0.025%) dopant [11]. Pegs4, which is used to create material in the EGSnrc package, was also used to construct TLD-100.

**Table 1:** Material depth where the TLD-100 chip was placed for considered media.

Phantom Materials	Density (g/cm <sup>3</sup> )	Depth (cm)	Beyond the depth of TLD-100 chip (cm)
Water	1.00	10	5
Polystyrene	1.06	9.43	4.72
Aluminum	2.7	3.71	1.85
Iron	7.87	1.27	0.64
Copper	8.96	1.12	0.56
Lead	11.35	0.88	0.44

For the particles' transport model, AE, AP, ECUT, and PCUT were characterized. AP and AE are the threshold energy for the production of photons and secondary electrons, respectively. ECUT and PCUT are used as cut-off energies for electron and photon transport, respectively. The parameters ECUT and AE were terminated at 0.7 MeV. The parameter AP and PCUT were set to 0.01 MeV. The parameter ESTEPE, which is fractional energy loss per electron step, was 2.5%. The parameters ESAVE is electron range rejection technique was set to 2 MeV and the parameter SBS, which is selective bremsstrahlung

splitting, were  $N_{min}=10$ ,  $N_{max}=100$ . SBS and ESAVE parameters were chosen for increasing simulation speed. A total 10<sup>7</sup> histories were simulated and statistical uncertainty was less than 1%.

**Cavity Theory**

*Tmax-based calculation*

Detectors (cavity) are used to measure dose in a medium. Generally, detector and medium have different atomic numbers and densities. The relationship between the  $D_{med}$  and the  $D_{cav}$  is given by Burlin's general cavity theory as follows:[12]

$$f = \frac{D_{cav}}{D_{med}} = d s / \rho_{med}^{cav} + (1 - d) \left( \frac{\mu_{en}}{\rho} \right)_{med}^{cav} \tag{1}$$

where  $f$  is known as the dose to the cavity to dose to the medium conversion factor. The parameter  $f$  varies with energy and radiation type. And also it varies with the size and composition of the cavity in the medium.  $\left( \frac{\mu_{en}}{\rho} \right)_{med}^{cav}$  is the ratio of average mass-energy absorption coefficients of the cavity to the medium and  $s / \rho_{med}^{cav}$  is the ratio of the mean mass collisional stopping power of the cavity to that of the medium. The parameter  $d$  is the weighting factor. It is related to cavity size and it is given by;

$$d \equiv \frac{\phi_m}{\phi_m^e} = \frac{\int_0^g \phi_m^e e^{-\beta l} dl}{\int_0^g \phi_m^e dl} = \frac{1 - e^{-\beta g}}{\beta g} \tag{2}$$

$$1 - d \equiv \frac{\phi_c}{\phi_c^e} = \frac{\int_0^g \phi_c^e (1 - e^{-\beta l}) dl}{\int_0^g \phi_c^e dl} = \frac{\beta g + e^{-\beta g} - 1}{\beta g} \tag{3}$$

where,  $\phi_m^e$  and  $\phi_m$  represent the electron fluence in medium with and without CPE (charged particle equilibrium), respectively.  $1-d$  is defined as the dose component resulting from photon interactions in the cavity. It is the ratio of the electron fluence created by the photons in the cavity to that created under electronic equilibrium [10].  $l$  represents the distance between a point in the cavity and the wall. The mean cord length, in other words, the average path length of electrons across the cavity is given by  $g$ ; often determined as;

$$g = \frac{4V}{S} \tag{4}$$

$V$  represents the cavity volume. The surface area of the cavity is given by  $S$ . Different sizes of TLD-100 dosimeters are used in clinical applications. The size of 0.32x0.32x0.09 cm<sup>3</sup> is frequently used in clinics. When the  $g$  parameter is calculated for these dimensions according to Eqn.4, the result is approximately 0.3[13]. In literature, the  $g$  parameter has been calculated for different TLD chip sizes using different equations [9,14]. This value ranges from 0.1 to 1 for the TLD-100 chip. To compare the results with the literature, the  $g$  value was chosen as 0.1, 0.3, 0.5, and 1.

$\beta$  represents the effective mass attenuation coefficient of the electrons. The electrons here are those that penetrate the cavity material originating from the wall. In the literature, different calculations have been made for  $\beta$ . There are many formulas proposed for calculating the value of  $\beta$  (see Table 2) from the maximum energy ( $T_{max}$ ) of the electron spectrum from a head-on Compton collision of a photon with energy  $h\nu$  or the extrapolated range ( $R$ ) of  $T_{max}$  [15].

$$T_{max} = \frac{2(h\nu)^2}{2h\nu + 0.511 \text{ MeV}} \quad (5)$$

Eqn. 5 is for monochromatic energy photon beams. For a 6 MV photon beam, the mean energy of the photons ( $h\nu_{mean}$ ) is approximately 1/3 of the kinetic energy of the incoming electrons [16]. In this study,  $h\nu_{mean}$  is chosen as 2 MeV. From Eqn. 5,  $T_{max}$  is 1.77 MeV.

**Table 2:** Equations for calculating  $\beta$ . The subscript number refers author of the study.

Author	Formula
Evans[17]	$\beta_1 = \frac{17}{(T_{max})^{1.14} \cdot 18 \cdot 6}$
Loevinger[18]	$\beta_2 = \frac{16}{(T_{max} - 0.036)^{1.37}}$
Burlin[12]	$\beta_3 = \frac{16}{(T_{max} - 0 \cdot 036)^{1.4}}$
Chan and Burlin[19]	$e^{(-\beta_4 R)} = 0.01$
Janssens[20]	$e^{(-\beta_5 R)} = 0.04$
Paliwal and Almond[21]	$\beta_6 = \frac{14}{(T_{max})^{1.09}}$

$f$  factor (Eqn.1) was calculated using the  $(\frac{\mu_{en}}{\rho})_{med}^{cav}$ , the  $s/\rho_{med}^{cav}$ , and the parameter  $d$ . The parameter  $d$  is obtained from  $\beta$  and  $g$  (Eqn.2).  $R$  and  $(\frac{\mu_{en}}{\rho})_{med}^{cav}$  are calculated from the  $h\nu_{mean}$  value [22] using NIST (National Institute of Standards and Technology) [23,24].  $s/\rho_{med}^{cav}$  is calculated from average equilibrium-spectrum electron energies ( $\frac{T_{av}}{2}$ ) [25]. The parameter  $T_{av}$  is given by:

$$\frac{T_{av}}{h\nu_{mean}} = \frac{\sigma_{tr}^e}{\sigma^e} \quad (6)$$

where  $\sigma_{tr}^e$  represents the energy transfer cross-section for Compton interaction.  $\sigma^e$  is the Klein-Nishina cross-section per electron [26]. To obtain  $\sigma_{tr}^e$  and  $\sigma^e$ , the literature was used [15]. In this part, the calculated  $f$  factors were named as  $f_{\beta_1}, f_{\beta_2}, f_{\beta_3}, f_{\beta_4}, f_{\beta_5}, f_{\beta_6}$  for Evans[17], Loevinger [18], Burlin [12], Chan and Burlin [19], Janssens [20] and Paliwal and Almond [21] equations, respectively.

**Spectrum weighted calculation**

Generally, the parameter  $\beta$  is assumed that the same for medium and cavity since it is the maximum energy of the spectrum which determines the  $\beta$  value. It is supposed that the electron spectra have the same maximum photon

energy in the medium and cavity [10]. However, the medium and the cavity have different materials. And the electron spectra are not identical. Therefore, Silva [10] suggests the following equations:

$$f = d(\frac{s}{\rho})_{med}^{cav} + d'(\mu_{en}/\rho)_{med}^{cav} \quad (7)$$

$$d' = \frac{1 - e^{-\beta_{avg} g}}{\beta_{avg}} \quad (8)$$

$$d'' = 1 - \frac{1 - e^{\beta'_{avg} g}}{\beta'_{avg}} \quad (9)$$

$\beta_{av}$  and  $\beta'_{av}$  represent the averaged values of the electron mass attenuation coefficients for the medium and cavity, respectively. The electron spectra were analyzed to calculate  $s/\rho_{med}^{cav}$ ,  $\beta_{av}$  and  $\beta'_{av}$ . The  $\beta$  values for each energy were obtained from Janssens [20] equation. The  $\beta$  and  $s/\rho$  were multiplied by the spectrum value corresponding to each energy to obtain the average effective mass attenuation coefficient and average mass collision stopping power, respectively. From full-spectrum, 0.04 MeV -  $T_{max}$  ((from eqn.5) = ~1.77 MeV) energy range was chosen to calculate these parameters.  $(\mu_{en}/\rho)_{med}^{cav}$  was calculated from humean. The value of  $f^{janssens}$  was calculated using Eqn. 7, 8, and 9.

**Results and Discussion**

In this study, to observe the electron spectrum effect on TLD-100 response in water, polystyrene, aluminium, iron, copper, and lead, the effective mass attenuation coefficient and mass collision stopping power were calculated using two different methods. Firstly, these parameters were calculated using the electron spectrum of the 6 MV photon beam in the aforementioned media. The electron spectra were obtained using BEAMnrc MC simulation with 0.1 % statistical error. Fig. 2 shows the electron energy versus spectrum from 0.01 to 6 MeV.

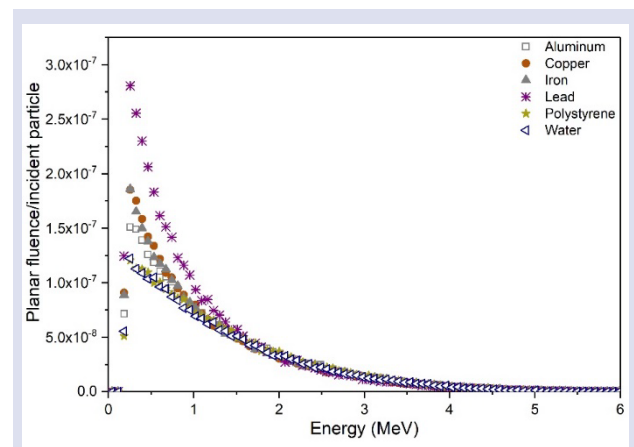


**Figure 2.** Planar electron spectral distribution of 6 MV photon beam in aluminum, copper, lead, iron, polystyrene, and water.

In the second method, the effective mass attenuation coefficient and mass collision stopping power were calculated from NIST [24] table using  $T_{max}$  ((from eqn.5) =  $\sim 1.77$  MeV) value. The electron ranges and mass collision stopping power have a 1 % relative error.

Table 3 presents the  $s/\rho$  obtained using spectrum weighted and NIST. It also presents mass energy-absorption coefficients.

**Table 3:** The  $(\mu_{en}/\rho)_{med}^{cav}$  and  $s/\rho_{med}^{cav}$  for TLD-100 chip dosimeter in the media studied, considering both the spectrum weighted and NIST

Medium	$(s/\rho)_{Material}^{TLD-100}$	$(s/\rho)_{Material}^{TLD-100}$	$(\mu_{en}/\rho)_{Material}^{TLD-100}$
	(from spectrum)	(NIST)	(NIST)
Water	0.808±1%	0.807	0.833
Polystyrene	0.827±1%	0.828	0.861
Aluminum	1.028±1%	1.029	0.959
Iron	1.156±1%	1.154	0.988
Copper	1.195±1%	1.196	1.006
Lead	1.548±1%	1.552	0.921

As seen in Table 3, the difference between the  $s/\rho_{med}^{TLD-100}$  from NIST and spectrum weighted approximation was no more than 0.3% for all media. The values of  $\beta$  were calculated using Table 1 and the results are shown in Table 4.

**Table 4:** Calculated  $\beta$  values, using Table 1, for the media considered.

$\beta$ (cm <sup>2</sup> g <sup>-1</sup> )	TLD-100	Water	Aluminum	Iron	Copper	Lead	Polystyrene
$B_1$	8.867	8.867	8.867	8.867	8.867	9.397	8.867
$B_2$	8.750	8.750	8.750	8.750	8.750	9.397	8.750
$B_3$	7.404	7.404	7.404	7.404	7.404	7.964	7.404
$B_4$	4.345	5.418	4.304	3.903	3.775	3.361	5.233
$B_5$	3.037	3.787	3.008	2.728	2.638	2.350	3.658
$B_6$	7.513	7.513	7.513	7.513	7.513	7.943	7.513

As seen in Table 4, the  $\beta$  values varied among themselves in the same material. While the  $\beta_{1-3}$  and  $\beta_6$  values did not change with material density except lead,  $\beta_4$  and  $\beta_5$  changed.  $\beta_{av}$  and  $\beta'_{av}$  were calculated using the spectrum of 6 MV photon beam. Table 5 displays  $\beta_{av}$  and  $\beta'_{av}$  values using spectrum weighted approximation for the TLD-100 chip which was in the considered media.

**Table 5:** The  $\beta_{av}$  and  $\beta'_{av}$  values were obtained using spectrum weighted approximation for the TLD-100 chip which was in the considered media.

Medium	$\beta_{av}$ and $\beta'_{av}$ (cm <sup>2</sup> g <sup>-1</sup> )	$\beta'_{av}$ (cm <sup>2</sup> g <sup>-1</sup> )
Water	16.819	13.612
Polystyrene	16.554	13.314
Aluminum	13.607	14.488
Iron	12.771	15.494
Copper	12.569	15.519
Lead	10.369	16.557

As seen in Table 5, while the value of  $\beta_{av}$  was more than  $\beta'_{av}$ , in water and polystyrene, it was the opposite for aluminum, iron, copper, and lead, and the maximum difference between the two parameters was seen in lead.

$d$  and  $1-d$  were calculated using Table 4 and Eqn.2-3 to obtain  $f_{\beta_1}, f_{\beta_2}, f_{\beta_3}, f_{\beta_4}, f_{\beta_5}, f_{\beta_6}$ .  $d'$  and  $d''$  were calculated using Table 5 and Eqn.8-9 for  $f^{d'anssens}$ . Table 6 shows the  $d$  and  $1-d$  values are considered media for  $g$  values from 0.1 to 1 gcm<sup>-2</sup>.

**Table 6:**  $d$  and  $1-d$  for different  $g$  (0.1, 0.3, 0.5, 1  $\text{g/cm}^2$ ) values using Eqns. 2-3 in considered media.

Medium	$g(\text{g/cm}^2)$							
	0.1		0.3		0.5		1.0	
	$d$	$1-d$	$d$	$1-d$	$d$	$1-d$	$d$	$1-d$
Water	0.83	0.17	0.60	0.40	0.45	0.55	0.26	0.74
Polystyrene	0.84	0.16	0.61	0.39	0.46	0.54	0.27	0.73
Aluminium	0.86	0.14	0.66	0.34	0.52	0.48	0.32	0.68
Iron	0.88	0.13	0.68	0.32	0.55	0.45	0.34	0.66
Copper	0.88	0.12	0.69	0.31	0.56	0.44	0.35	0.65
Lead	0.90	0.10	0.74	0.26	0.62	0.38	0.42	0.58

Table 7 shows the  $d'$  and  $d''$  for different  $g$  (0.1, 0.3, 0.5, 1  $\text{g/cm}^2$ ) values using Eqn. 8-9 in media considered

**Table 7:**  $d'$  and  $d''$  for different  $g$  (0.1, 0.3, 0.5, 1  $\text{g/cm}^2$ ) values using Eqns. 8-9 in considered media.

Medium	$g(\text{g/cm}^2)$							
	0.1		0.3		0.5		1.0	
	$d'$	$d''$	$d'$	$d''$	$d'$	$d''$	$d'$	$d''$
Water	0.49	0.45	0.20	0.76	0.12	0.85	0.06	0.93
Polystyrene	0.49	0.45	0.20	0.75	0.12	0.85	0.06	0.93
Aluminium	0.55	0.47	0.24	0.77	0.15	0.86	0.07	0.93
Iron	0.57	0.49	0.26	0.79	0.16	0.87	0.08	0.94
Copper	0.57	0.49	0.26	0.79	0.16	0.87	0.08	0.94
Lead	0.62	0.51	0.31	0.80	0.19	0.88	0.10	0.94

As seen in Table 6 and 7, the  $d$  and  $d'$  decreases while the  $1-d$  and  $d''$  increases as the cavity gets larger. Values in both tables are also affected by the density of the media. The parameters have maximum values in lead.

Fig. 3 shows that the  $f$  values for the TLD-100 chip in considered media as a function of  $g$ .

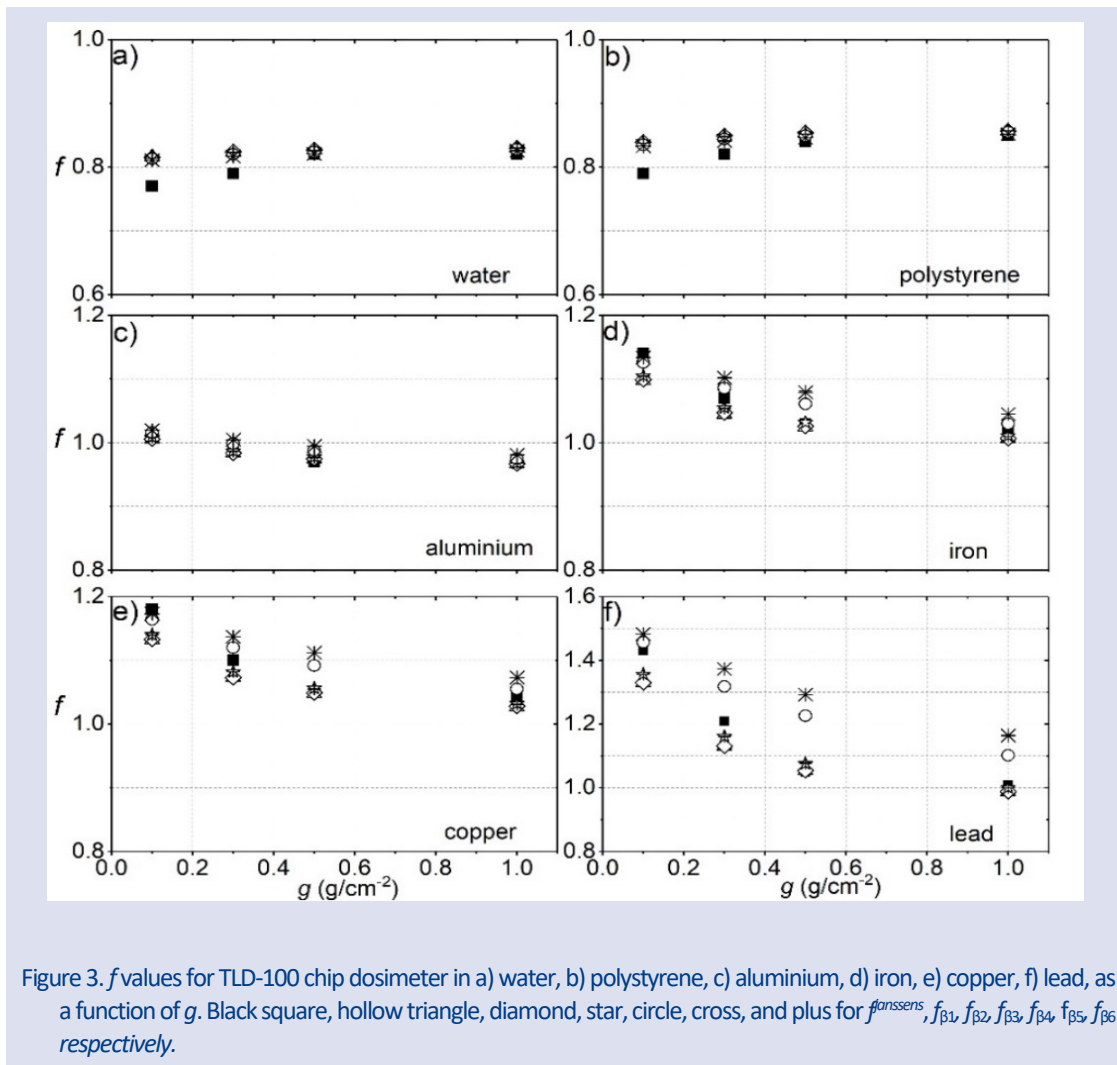


Figure 3.  $f$  values for TLD-100 chip dosimeter in a) water, b) polystyrene, c) aluminium, d) iron, e) copper, f) lead, as a function of  $g$ . Black square, hollow triangle, diamond, star, circle, cross, and plus for  $f_{\text{amssens}}$ ,  $f_{\beta 1}$ ,  $f_{\beta 2}$ ,  $f_{\beta 3}$ ,  $f_{\beta 4}$ ,  $f_{\beta 5}$ ,  $f_{\beta 6}$  respectively.

The estimated relative errors in this study are  $\mu_{en}/\rho$  (2%),  $s/\rho$  (1%), and  $R$  (1%) [24]. This relative error is less than 3% in the calculated  $f$  values. As seen in Fig. 3, when the density of the medium increased, the  $f$  values increased. The  $f$  values were affected by the density of the medium. The  $f$  values were very close to each other in the same media except lead despite the  $\beta$  values being very different from each other. The standard deviation between  $f$  values was less than 2.5% except lead for different  $g$  (0.1, 0.3, 0.5 and 1 g/cm<sup>2</sup>) values. It was 5.6%, 9%, 9%, 6.2% for 0.1, 0.3, 0.5 and 1 g/cm<sup>2</sup>, respectively. In the literature, the difference between  $f$  values for <sup>60</sup>Co gamma-rays is not more than 5% in lead.

## Conclusion

In this study, the Burlin General Cavity Theory was applied to obtain the response of the TLD-100 chip to 6 MV in different media using two different methods.  $T_{max}$ -based calculations and the electron spectrum weighted were used to calculate the response of the TLD-100 chip. At 6 MV, the maximum difference between the  $f$  values obtained using the two methods was about 10 % for lead, while it was less than 2.5 % for other media. The results indicated that the differences between  $f$  factors calculated using these two methods were insignificant except for lead. When the energy was increased from <sup>60</sup>Co to 6 MV photon beam, the difference between  $f$  values calculated from the two methods increased for lead material. It was shown that the  $f$  values increased as the density of the medium increased.

## Conflicts of interest

The authors state that did not have a conflict of interests.

## References

- [1] Chen R. and Leung P. L., Nonlinear dose dependence and dose-rate dependence of optically stimulated luminescence and thermoluminescence, *Radiation Measurements*, 33 (5) (2001) 475-481.
- [2] Montañó-García C. and Gamboa-deBuen I., Measurements of the optical density and the thermoluminescent response of LiF:Mg,Ti exposed to high doses of <sup>60</sup>Co gamma rays, *Radiation Protection Dosimetry*, 119 (1-4) (2006) 230-2.
- [3] Hsi W. C., Fagundes M., Zeidan O., Hug E., and Schreuder N., Image-guided method for TLD-based in vivo rectal dose verification with endorectal balloon in proton therapy for prostate cancer, *Medical Physics*, 40 (5) (2013) 051715.
- [4] Liuzzi R., Savino F., D'Avino V., Pugliese M., and Cella L., Evaluation of LiF:Mg,Ti (TLD-100) for Intraoperative Electron Radiation Therapy Quality Assurance, *PLoS ONE*, 10 (10) (2015) 0139287.
- [5] Carlsson G. A., Theoretical Basis for Dosimetry, 1 st ed. USA: Academic Press, Inc., (1985) 2-77.
- [6] Haraldsson P., Knöös T., Nyström H., and Engström P., Monte Carlo study of TLD measurements in air cavities, *Physics in Medicine and Biology*, 48 (18) (2003) 253-9.
- [7] Ma C. M. and Li J., Dose specification for radiation therapy: Dose to water or dose to medium?, *Physics in Medicine and Biology*, 56 (10) (2011) 3073-89.
- [8] Alashrah S., Kandaiya S., Maalej N., and El-Taher A., Skin dose measurements using radiochromic films, TLDs and ionisation chamber and comparison with Monte Carlo simulation, *Radiation Protection Dosimetry*, 162 (3) (2014) 338-44.
- [9] Mobit P. N., Nahum A. E., and Mayles P., An EGS4 Monte Carlo examination of general cavity theory An EGS4 Monte Carlo examination of general cavity theory, *Physics in Medicine and Biology*, 42 (7) (1997) 1319-34
- [10] Silva H., An analysis of the electron spectrum effect on LiF response to cobalt-60 gamma-rays, *Nuclear Inst. and Methods in Physics Research B*, 44 (1989) 166-171.
- [11] Davis S. D., High Sensitivity Lithium Fluoride As a Detector for Environmental Dosimetry, M.Sc Thesis, McGill University, Medical Physics Unit, (2003).
- [12] Burlin T. E., A general theory of cavity ionisation, *The British Journal of Radiology*, 39 (466) (1966) 727-34.
- [13] Sarigül N., Surucu M., Reft C., Yegingil Z., and Aydogan B., Examination of general cavity theory for magnesium and titanium doped lithium fluoride (TLD-100) of varying thicknesses in bone and lung, *Radiation Measurements*, 94 (2016) 1-7.
- [14] Horowitz Y. S., Photon general cavity theory, *Radiation Protection Dosimetry*, 9 (1) (1984) 5-18.
- [15] Attix F. H., Introduction to Radiological Physics and Radiation Dosimetry, 2nd ed. New York: Wiley-VCH, (1986).
- [16] Edwards C. R. and Mountford P. J., Near surface photon energy spectra outside a 6 MV field edge, *Physics in Medicine and Biology*, 49 (18) (2004) 293-301.
- [17] Evans R. D., The Atomic Nucleus, 1 st edition, New Delhi: Tata McGraw-Hill, (1955).
- [18] Loevinger R., The dosimetry of beta sources in tissue; the point-source function, *Radiology*, 66 (1) (1956) 55-62.
- [19] Burlin T. E. and Chan F. K., The effect of the wall on the Fricke dosimeter, *The International Journal of Applied Radiation and Isotopes*, 20 (11) (1969) 767-775.
- [20] Janssens A., Eggermont G., Jacobs R., and Thielens G., Spectrum perturbation and energy deposition models for stopping power ratio calculations in general cavity theory, *Physics in Medicine and Biology*, 19 (5) (1974) 619-30.
- [21] Paliwal B. R. and Almond P. R., Applications of cavity theories for electrons to LiF dosimeters, *Physics in Medicine and Biology*, 20 (4) (1975) 547-58.
- [22] Podgorsak E. B. and Kainz K., Radiation Oncology Physics: A Handbook for Teachers and Students, *Medical Physics*, 33 (6) (2006) 1920.
- [23] Berger M.J., Coursey J.S., Zucker M.A., and Chang J., ESTAR, PSTAR, and ASTAR: Computer Programs for Calculating Stopping-Power and Range Tables for Electrons, Protons, and Helium Ions (version 1.2.3), National Institute of Standards and Technology, Available at: <http://physics.nist.gov/PhysRefData/Star/Text/ESTAR.html> Retrieved April 7, 2022.
- [24] Hubbel J. H. and Seltzer S. M., Tables of X-Ray Mass Attenuation Coefficients and Mass Energy-Absorption Coefficients (version 1.4), National Institute of Standards and Technology, Available: <https://www.nist.gov/pml/x-ray-mass-attenuation-coefficients> Retrieved April 7, 2022
- [25] Bull R. K., Stopping powers for electrons and positrons, *International Journal of Radiation Applications and Instrumentation. Part D. Nuclear Tracks and Radiation Measurements*, 11 (4-5) (1986) 273.
- [26] Horowitz Y. S., The theoretical and microdosimetric basis of thermoluminescence and applications to dosimetry., *Physics in Medicine and Biology*, 26 (5) (1981) 765-824.